Simulation on photovoltaic device

Submitted By

Rahul Pal

Roll No.308036

Registration No. VB-829 2021-22

Under supervision of

Dr. Swapan K. Mandal

For the Fulfilment of M. Sc. Semester-IV Dissertation Paper

Department of Physics

Visva-Bharati, Santiniketan

May 2023

Certificate from Supervisor

This is to certify that the dissertation work entitled "Simulation on photovoltaic device" has been undertaken and written under my supervision and it describes the original work carried out by Rahul Pal for the partial fulfilment of M.Sc. degree.

Date: _____

Dr. Swapan K. Mandal

Department of Physics

Siksha-Bhavana

Visva-Bharati, Santiniketan

Contents

Table of Figures:

Abstract:

In the modern era, it is a challenge to meet the enormous energy demand of our everyday life solely based on fossil fuels. Thus, developing smart and useful materials which transforms light into usable energy are the most investigated research methods for the generation of renewable energy source. In the field of photovoltaics, perovskite solar cells (PSC) have been called a game-changer. With the enormous advancement in perovskite solar cells' power conversion efficiency (PCE), which increased from 3.8% to 25% in few years. In our work we have given a brief introduction to charge generation and charge transport in perovskite solar cells and the underlaying physics of it. To simulate the physical properties of the solar cell we have used Solar Cell Capacitance Simulator (SCAPS-1D) application and the numerical methods related to this is also briefly discussed initially. Next, an organic-inorganic mixed single perovskite $CH_3NH_3PbI_3$ material is employed as an active layer for solar cell fabrication and (SCAPS-1D) was used to study the device configuration Glass/ITO/WS_2/$CH_3NH_3PbI_3$/P3HT/Au. The device performance is investigated by varying the solar cell active layer thickness, bandgap, doping concentration and temperature. Further, using the optimal value of the different parameters, the performance of the photo-voltaic device such as power conversion efficiency (PCE) and Fill Factor (FF) are obtained as 28.38%, and 90.93%, respectively. Also, Open-circuit voltage (V_{OC}) of 1.4275 V and short-circuit current density (J_{SC}) of 21.86 mA cm^{-2} were achieved. The effect of donor concentrations has been investigated by changing its value for the proposed device from 1×10^{-12} cm^{-3} to 1×10^{-20} cm^{-3}. The power convergence efficiency of the perovskite solar cell has therefore been improved by the use of several charge transport materials. Our simulation analysis demonstrates that the suggested design might be used to create a device for enhancing the effectiveness of the perovskite solar cell.

Introduction

As is well known, traditional fossil fuels are presently necessary. And all of the industrial revolutions have brought in an unrecognised period of economic growth for modern culture, increasing the conflict between man and nature while also caused massive consumption of resources and energy. As a result, we currently face a heavy environmental and ecological price. The need for energy has increased quickly along with the rapid expansion of our daily social lives, and conventional fossil fuels are unable to keep up with our needs. Hence, there is a global crisis involving energy and resources, the environment, ecology, and climate change nowadays. These issues collectively are what started the fourth industrial revolution, which is also known as the green industrial revolution. Due to its advantages of being pollution-free, renewable, having a large amount of energy, etc., solar energy is currently becoming a new support for human and social development. The formula ABX_3 represents (Figure 1) the perovskite crystal structure where A is a large organic or inorganic cation, B is a smaller inorganic cation such as (Cu^{2+}, Sn^{2+}, Pb^{2+}) and X_3 is anion from the halogen group (such as Cl^-, Br^- and I^-) that is able to bond with both cations A and B. [1]

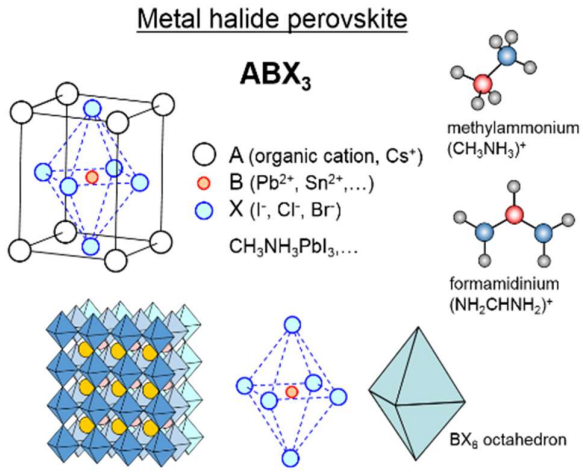

Figure 1. Structure of metal halide perovskites

Haloalkanes perovskite and organic-inorganic halide perovskite are the two primary kinds of perovskite crystal structure, respectively. Due to its superior optoelectronic properties and high absorption coefficients, perovskite materials are a more effective alternative to silicon and work well as the absorber layer in solar applications. Another important characteristic is their ferroelectric behaviour[2–6]

which was discovered half a century ago[7]. PSCs also have the added benefits of low-cost manufacturing at moderate temperatures, a direct band gap, reduced exciton binding energy, and improved light absorption capabilities [8]. High values of PCE, Fill Factor, Short Circuit Current Density, and Open Circuit Voltage are required for a cost-effective solar cell in order to directly convert a sizable portion of incident solar energy into electrical energy via the photovoltaic effect.

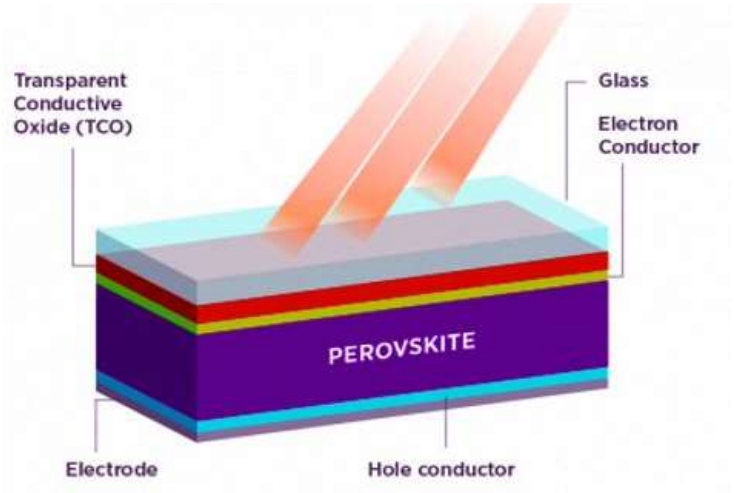

Figure 2. Schematic diagram of Perovskite Solar cell

The power conversion efficiency (PCE) of PSCs based on lead (Pb) perovskites has been improved from the initial 3.8% to the recently certified value of 25.2 % [9]. The perovskite (absorber) is positioned between the electron transport layer and the hole transport layer (Figure 2) in a standard perovskite solar cell. To construct perovskite solar cells with good performance, materials for ETL and HTL with excellent active layers are extremely valuable [10]. A theoretical study [11] of the various parameters has been carried out, and the results for the photovoltaic parameters of the devices such as short circuit current density (Jsc), open-circuit voltage (V_{OC}), fill factor (FF), and power conversion efficiency (PCE) are examined. The maximum current density refers to the maximum amount of electric current that can flow through a given cross-sectional area of a material. Open circuit voltage or V_{oc} refers to the voltage that is present in a circuit when there is no current flowing through it. It is the voltage that a voltage source, such as a battery or generator, will produce when it is not connected to a load or other circuit components. It is the maximum voltage a solar cell is capable of producing. Fill factor (FF) is a parameter that is used

to describe the efficiency of a solar cell or photovoltaic (PV) module. It represents the ratio of the maximum power that can be obtained from the cell or module to the product of the open circuit voltage and short circuit current. Power conversion efficiency (PCE) is a measure of the ability of a device, such as a solar cell or a battery, to convert input power into useful output power. It is defined as the ratio of the output power to the input power, expressed as a percentage: PCE = (output power / input power) x 100%.

The construction of the device using various ETL and HTL in addition to $CH_3NH_3PbI_3$ as the perovskite material has already been published. To the best of the evidence relating, WS_2 as an ETL material with $CH_3NH_3PbI_3$ as a perovskite material has not yet been observed for the enhancement of device performance in PSC. In the current study, WS2 as an ETL and P3HT as HTL have been taken with $CH_3NH_3PbI_3$ for the fabrication of the PSC first time. The PCE of the present device is 28.83%. By using the WS2 as an ETL material and P3HT as an HTL material for the perovskite ($CH_3NH_3PbI_3$), we got the maximum device parameters i.e., V_{OC}, J_{SC}, FF and PCE. In the present work, Glass/ITO/WS_2/$CH_3NH_3PbI_3$/P3HT/Au was investigated using the SCAPS-1D simulator program. SCAPS-1D Software developed at the University of Gent Belgium in 2018 is used for the simulation in the present work [12]. A sufficient response on the solar cell characteristics for $CH_3NH_3PbI_3$ has led to the use of WS2 as an ETL and P3HT as an HTL in the planned device configuration. Transferring the charge carriers created by the device's active layer's absorption of solar radiation to the Electron Transport Layer (ETL) and Hole Transport Layer (HTL) is their primary purpose[13–16]. Bandgap, doping concentration, temperature, and other parameters have been adjusted and modified to improve the performance of photovoltaic solar cells. More specifically, the efficiency (PCE) and fill-factor (FF) of the suggested device are obtained at 27.02% [8,13,17] and 85.44 %, respectively, utilising the ideal values of the various parameters. Thus, the power conversion efficiency (PCE) of the perovskite solar cell has been improved by using various charge transport materials. There are four sections in this work. Section 1 puts out an outline of the solar cell. In section 2, We discuss the Perovskite solar cell device's functionality and layered construction and numerical method. The impact of replacing the absorber layer is shown in section 3 along with thickness, and bandgap. acceptor density and temperature analysis of the solar devices, and section 4 concludes the present study.

Solar Cell Physics

Solar cells also known as photovoltaic cells, convert sunlight directly into electricity through the photovoltaic effect. The photovoltaic effect is a process by which photons (light particles) collide with electrons in a material, causing them to be excited and break free from their atoms. These free electrons can then flow through the material as an electrical current. The basic structure of a solar cell consists of a thin layer of a semiconductor material, such as silicon, that is sandwiched between two layers of differently-doped semiconductors. The semiconductor material is chosen because it has a bandgap that allows it to absorb sunlight and create free elect Solar cells, also known as photovoltaic cells, convert sunlight directly into electricity through the photovoltaic effect. The photovoltaic effect is a process by which photons (light particles) collide with electrons in a material, causing them to be excited and break free from their atoms. These free electrons can then flow through the material as an electrical current. The basic structure of a solar cell consists of a thin layer of a semiconductor material, such as silicon, that is sandwiched between two layers of differently-doped semiconductors. The semiconductor material is chosen because it has a bandgap that allows it to absorb sunlight and create free electrons and holes (positive charges left behind by the free electrons). When photons from sunlight hit the solar cell, they are absorbed by the semiconductor material and create free electrons and holes. The electric field in the junction between the two differently-doped layers of the solar cell then separates the free electrons and holes, pushing them to opposite sides of the cell. The separated electrons flow through an external circuit, producing an electrical current, while the holes flow in the opposite direction.

To improve the efficiency of solar cells, various techniques are used to reduce the amount of energy lost as heat. For example, anti-reflection coatings can be applied to the surface of the solar cell to reduce reflection and increase the amount of sunlight absorbed. Additionally, multi-junction solar cells can be used, which consist of multiple layers of semiconductors with different bandgaps that can absorb different wavelengths of light. ions and holes (positive charges left behind by the free electrons).

When photons from sunlight hit the solar cell, they are absorbed by the semiconductor material and create free electrons and holes. The electric field in the junction between the two differently-doped layers of the solar cell then separates the

free electrons and holes, pushing them to opposite sides of the cell. The separated electrons flow through an external circuit, producing an electrical current, while the holes flow in the opposite direction.

A photodetector and a solar cell vary qualitatively in four ways:

1. A photodiode works on a narrow range of wavelength other hand solar cells need to work over a broad spectral range (solar spectrum).
2. To optimise exposure, solar cells are typically large-area devices.
3. Solar cells are frequently large-area devices in order to maximise exposure.
4. Quantum efficiency, which describes signal-to-noise ratio in photodiodes, is the relevant metric, whereas power conversion efficiency, which measures power delivered per incident solar energy, is relevant for solar cells. Normally, the external load that solar cells are attached to and the solar cells themselves are built to optimise the power delivered.

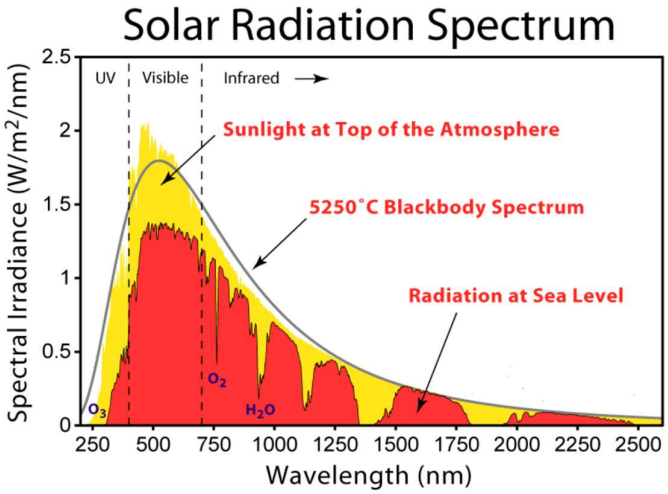

Figure 3 : Typical solar spectrum at the top of the atmosphere and at sea level. The difference is the radiation absorbed/scattered by the atmosphere. The spectrum of a black body at 5250°C is also superimposed and used for modelling. Modified from http://en.wikipedia.org/wiki/Sunlight

Solar Spectrum

The normal solar spectrum ranges in wavelength from 3 μm to 0.2μm, from the infrared to the ultraviolet. However, the intensity varies. As shown in the plot of spectral irradiance vs. wavelength for a typical solar spectrum, is shown in Figure *3*. The area under the curve gives the total areal intensity and this is approximately 1.35 kW m^{-2}. A black body radiation curve can roughly represent the sun spectrum at a temperature of 5250 °C. The scattering and absorption caused by the atmosphere can also be seen in the difference between the spectra obtained at the surface and at the top of the atmosphere. The angle of the light in the atmosphere, which changes depending on the time of day, determines its path length. The air mass number (AM), which is the secant of the angle between the sun and the zenith (secθ), provides this information. The sun spectrum outside of the earth's atmosphere is represented by AM0.The AM**1** phase has an intensity of 0.925 kW m^{-2} and occurs when the angle is zero, or when the sun is at its zenith. AM2 is when sun is at angle of 60° and its intensity is 0.691 kW m-2. The different spectra are plotted in Figure *4*.

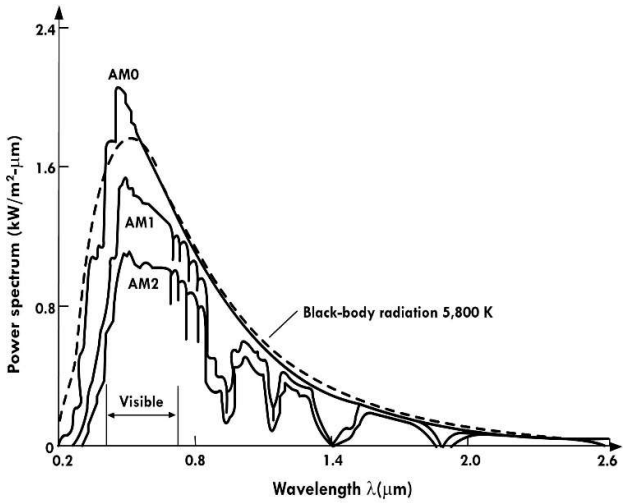

Figure 4: Typical solar spectrum for different air mass conditions. The plot shows AM0 (spectrum outside the atmosphere), AM1 (at the zenith), and AM2 (at an angle of 60°). This again can be modelled by black body spectrum, at various temperatures. Adapted from Physics of semiconductor devices - S.M. Sze.

The data can also be plotted as a photon flux density i.e. number of photons per unit energy per unit area per unit time. This is shown in Figure 5 .

Solar cell working principle

A simple solar cell is a *pn* junction diode. The schematic of the device is shown in Figure *6*. The *n* region is heavily doped and thin so that the lightcan penetrate through it easily. The *p* region is lightly doped so that most of the depletion region lies in the *p* side. The penetration depends on the wave- length and the absorption coefficient increases as the wavelength decreases. Electron hole pairs (EHPs) are mainly created in the depletion region and dueto the built-in potential and electric field, electrons move to the *n* region and the holes to the *p* region. When an external load is applied, the excess electrons travel through the load to recombine with the excess holes. Electronsand holes are also generated with the *p* and *n* regions, as seen from Figure *6*. The shorter wavelengths (higher absorption coefficient) are absorbed in the*n* region and the longer wavelengths are absorbed in the bulk of the *p* re gion. Some of the EHPs generated in these regions can also contribute to the current. Typically, these are EHPs that are generated within the minority

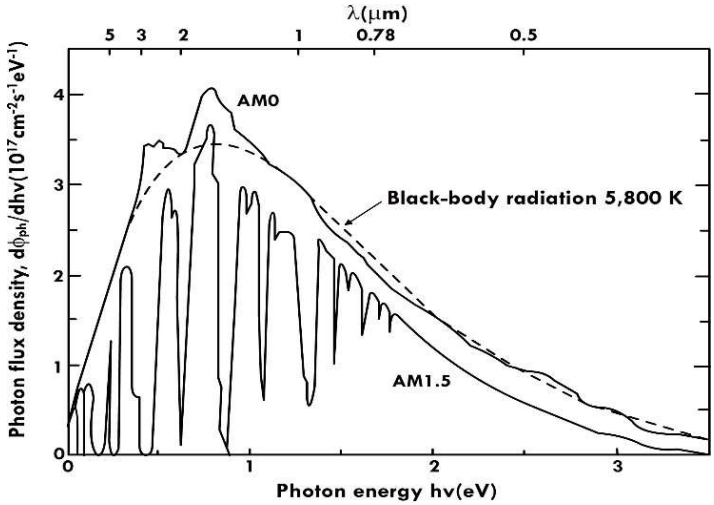

Figure 5 : Solar spectrum plotted as photon flux density vs. energy for AM0 and AM1.5. The difference in the spectra is due to the absorption/scatteringby the atmosphere. Adapted from Physics of semiconductor devices - S.M. Sze.

carrier diffusion length, L_e for electrons in the *p* side and L_h for holes in the *n* side. Carriers produced in this region can also diffuse into the depletion region and contribute to the current. Thus, the total width of the region that contributes to the solar cell current is $w_d+L_e+L_h$, where w_d is the depletion width. This is shown in Figure *7*. The carriers are extractedby metal electrodes on either side. A finger electrode is used on the top to make the electrical contact, so that there is sufficient

surface for the light topenetrate. The arrangement of the top electrode is shown in Figure 8 .

Consider a solar cell made of Si. The band gap, E_g, is 1.1 eV so that wavelength above 1.1 μm is not absorbed since the energy is lower than the band gap. Thus, any λ greater than 1.1 μm has negligible absorption. For λ much smaller than 1.1 μm the absorption coefficient is very high and the EHPs are generated near the surface and can get trapped near the surface defects. So, there is an optimum range of wavelengths where EHPs can contribute to photocurrent, shown in Figure 7.

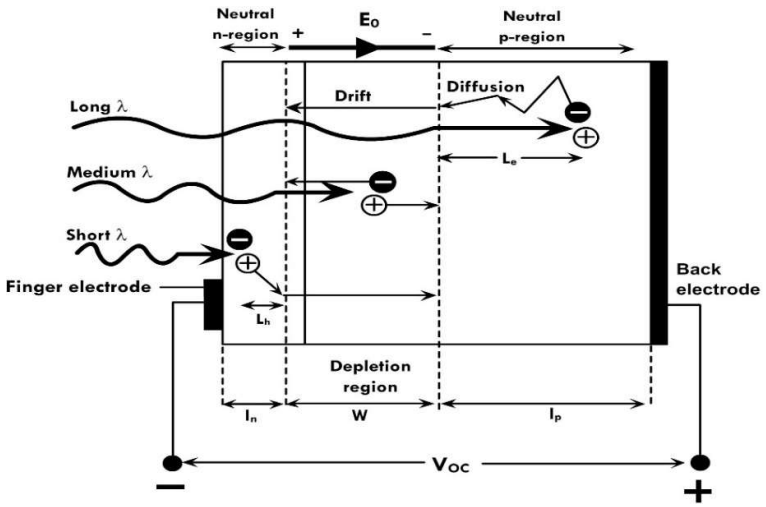

Figure 6. Principle of operation of a pn junction solar cell. Radiation is absorbed in the depletion region and produces electrons and holes. Theseare separated by the built-in potential. Depending on the wavelength and the thickness different parts of the device can absorb different regions of the solar spectrum. Adapted from Principles of Electronic Materials - S.O. Kasap

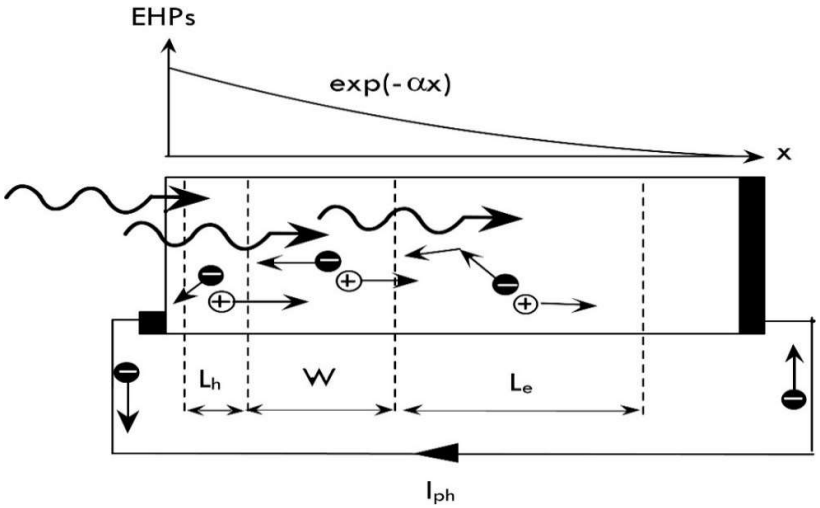

Figure 7. Photogenerated carriers in a solar cell due to absorption of light. w is the width of the depletion region, while L_h and L_e are minority carrier diffusion lengths in the n and p regions. The amount of absorption reduces with depth and hence the depletion region must be close to the surface to maximize absorption. This is achieved by having a thin n region. Adapted from Principles of Electronic Materials - S.O. Kasap

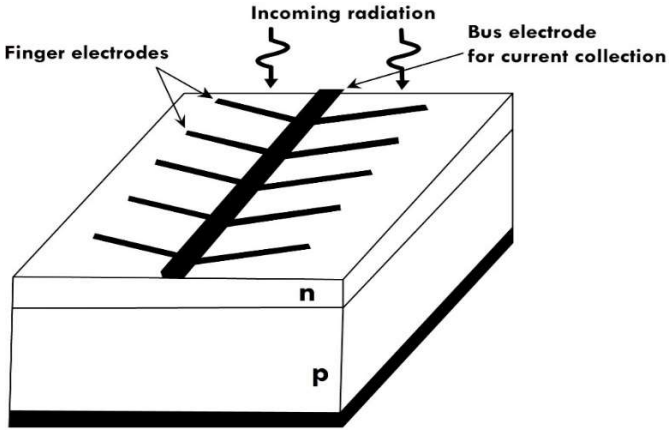

Figure 8. Finger electrodes on a pn junction solar cell. The design consists ofa single bus electrode for carrying current and finger electrodes that are thin enough so that sufficient light can be absorbed by the solar cell. Adapted from Principles of Electronic Materials - S.O. Kasap

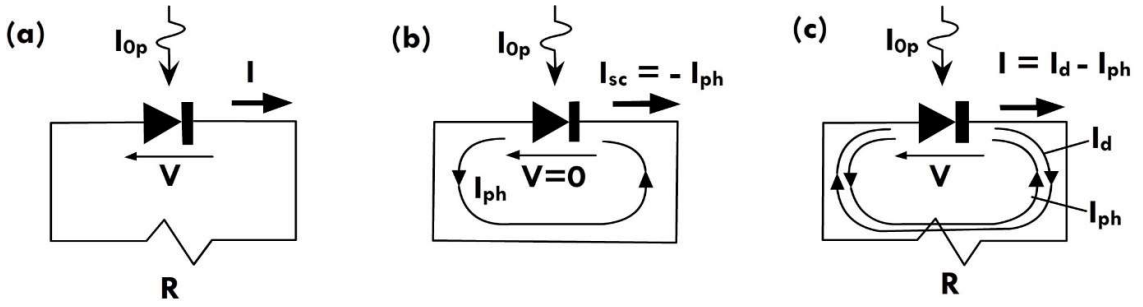

Figure 9. (a) pn junction solar cell under illumination with an external load. The equivalent circuit (b) without and (c) with an external load. The illumination causes a photocurrent to flow through the external circuit. When an external load is applied the potential drop across it creates a forward bias current, that opposes the photocurrent. Adapted from Principles of Electronic Materials - S.O. Kasap

Solar cell I-V characteristics

It possible to calculate the I-V characteristics of the solar cell by considering its equivalent circuit. The I-V characteristics depend on the intensity of the incident radiation and also the operating point (external load) of the cell. Consider a *pn* junction solar cell under illumination, as shown in Figure 9. If the external circuit is a short circuit (external load resistance is zero) then the only current is due to the generated EHPs by the incident light. This is called the photocurrent, denoted by I_{ph}. Another name for this is the *short circuit current*, I_{sc}. By definition of current, this is opposite to the photo current and is related to the intensity of the incident radiation, I_{op}, by

$$I_{sc} = -I_{ph} = -kI_{op} \qquad (1)$$

where k is a constant and depends on the particular device. k is equivalent to an efficiency metric that measures the conversion of light into EHPs. Consider the case when there is an external load R, as shown in *Figure 9*. The equivalent circuit for this case is shown in Figure 10. There is a voltage across the external load, given by $V=IR$. This voltage opposes the builtin potential and reduces the barrier for carrier injection across the junction.This is similar to a *pn* junction in forward bias, where the external bias causes injection of minority carriers and increased current. This forward bias current opposes the photo current generated within the device

due tothe solar radiation. This is because I_{ph} is generated due to electrons going to the n side and holes to the p side due to the electric field within the device, i.e. *drift current* while the forward bias current is due to *diffusion current*

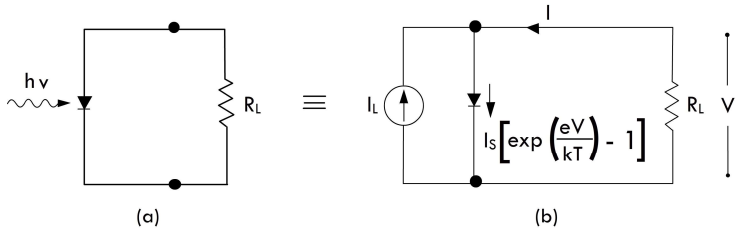

Figure 10. (a) A solar cell connected to an external load (b) Equivalent circuit, with a constant current source, a forward biased pn junction and the externalload. The current from the forward biased pn junction opposes the constant current source.

caused by the injection of minority carriers. Thus, the net current can be written as

$$I_d = -I_{ph} + I_d$$

$$I_d = I_{s0}\left[exp\left(\frac{eV}{k_B T}\right) - 1\right] \qquad (2)$$

$$I = -I_{ph} + I_{s0}\left[\exp\left(\frac{eV}{k_B T}\right) - 1\right]$$

where I_d is the forward bias current and can be written in terms of the reverse saturation current, I_{so} and external voltage V. The overall I-V characteristics is plotted in *Figure 11*.

In the absence of light, the *dark characteristics* is similar to a *pn* junction I-V curve. The presence of light (I_{ph}) has the effect of shifting the I-V curve down. From *Figure* 11. it is possible to define a photo current I_{ph}, which is the current when the external voltage is zero and an *open circuit voltage*, V_{oc}, which is the voltage when the net current in the circuit is zero. Using equation (2)V_{oc} can be calculated as

$$I_{ph} = I_{s0}\left[exp\left(\frac{eV}{k_B T}\right) - 1\right]$$

$$V_{oc} \approx \frac{k_B T}{e} ln\,[\frac{I_{ph}}{I_{s0}}] \qquad (3)$$

Higher the photon flux, higher is the value of I_{ph} (by equation (1) and higher the value of V_{oc}. Similarly, lower I_{so} can also cause higher V_{oc}. Since I_{so} isthe reverse

saturation current for the *pn* junction it is given by

$$I_{s0} = n_i^2 e \left[\frac{D_e}{L_e N_A} + \frac{D_h}{L_h N_D}\right] \tag{4}$$

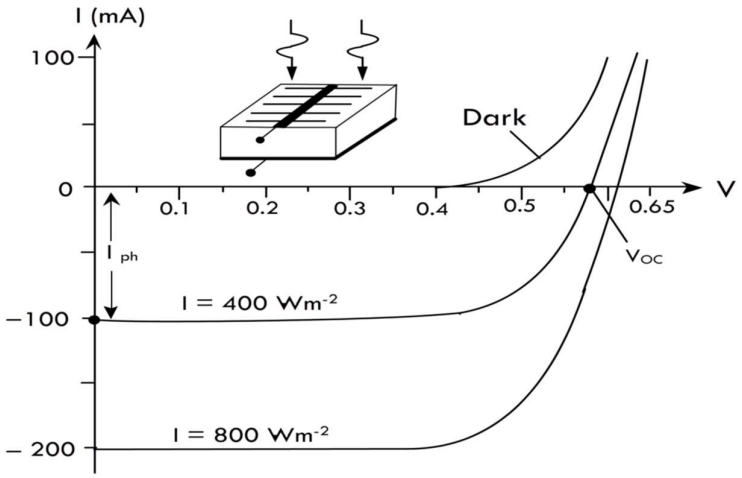

Figure 11. I - V characteristics of Si pn junction solar cell under dark conditions and under illumination with light of increasing intensity. Short circuit current and open circuit voltage both increase with increasing illumination. Adapted from Principles of Electronic Materials - S.O. Kasap

The reverse saturation current can be lowered by choosing a material with a higher band gap, E_g, which will cause ni to be lower. But this will also reduce the range of wavelengths that can be absorbed by the material, which will have the effect of lowering I_{ph}. The total power in the solar cell circuit is given by

$$P = IV = I_{s0}V\left[exp\left(\frac{eV}{k_B T}\right) - 1\right] - I_{ph}V \tag{5}$$

For maximum power, its derivative with respect to voltage should be zero. This gives a recursive relation in current and voltage.

$$\frac{dP}{dV} = 0$$

$$I_m \approx I_{ph}\left(1 - \frac{k_B T}{eV_m}\right)$$

$$V_m \approx V_{oc} - \frac{k_B T}{e} ln\left(1 + \frac{eV_m}{k_B T}\right)$$

$$P_m = I_m V_m \approx I_{ph}\left[V_{oc} - \frac{k_B T}{e}\ln\left(1 + \frac{eV_m}{k_B T}\right) - \frac{k_B T}{e}\right] \quad (6)$$

This can be seen from Figure 12. The area under the curve, corresponding to I_m and V_m, gives the maximum power. From equation (6) it can be seen that the maximum power is directly proportional to V_{oc} and can be increased by decreasing I_{so}. This means that smaller n_i and a larger E_g are favourable but the trade-off is that less radiation is absorbed.

Solar cell materials and efficiency

Conventional solar cells are made of Si single crystal and have an efficiency of around 22-24%, while polycrystalline Si cells have an efficiency of 18%. A schematic representation of such a cell is shown in Figure 8. The efficiency of the solar cell depends on the band gap of the material and this is shown in Figure *13*. Polycrystalline solar cells are cheaper to manufacture but have a lower efficiency since the microstructure introduces defects in the material that can trap carriers. Amorphous solar cells have an even lower efficiency but can be grown directly on glass substrates by techniques like sputtering so that the overall cost of manufacturing is lowered. There are also design improvements in the solar cell that can enhance the efficiency. PERL (passivated emitter rear locally diffused) cells, shown in Figure *14*, have an efficiency of 24% due to the inverted pyramid structure etched on the surface that enhances absorption.

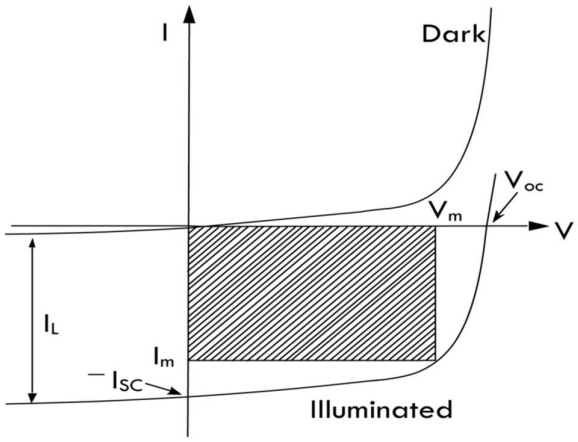

Figure 12. I-V curve for a solar cell with maximum power indicated by the shaded area. The corresponding voltage and current are V_m and I_m. The value depends on the external load applied. Adapted from Physics of semiconductor devices - S.M. Sze.

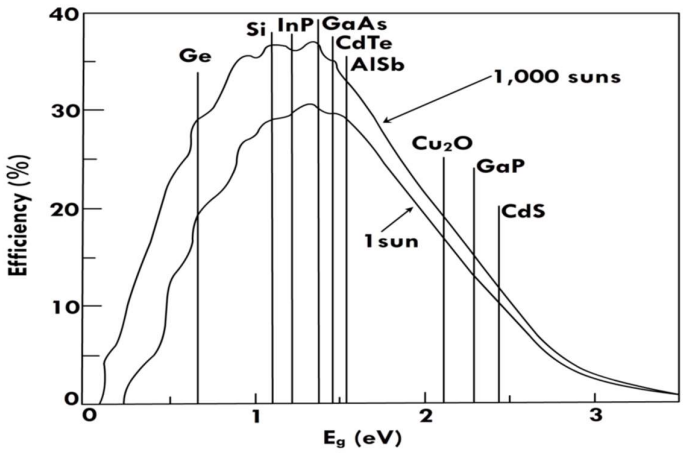

Figure 13. Solar cell efficiency as a function of band gap of the semiconductor material. There is a particular band gap range where the efficiency is maximum. Adapted from Physics of semiconductor devices - S.M. Sze.

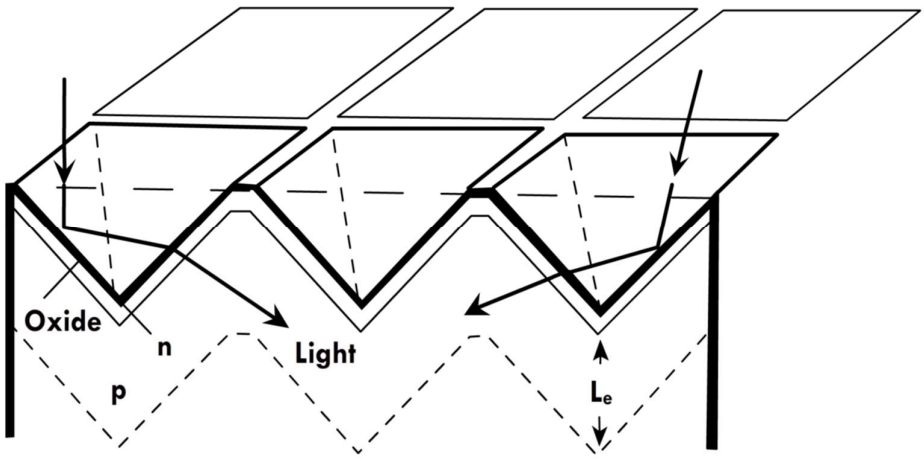

Figure 14. Si solar cell with an inverted pyramid structure to enhance absorption of the incoming radiation. These are called PERL cells. The inverted pyramid structure causes multiple reflections at the surface, which help in absorption of the incoming radiation. Adapted from Principles of Electronic Materials - S.O.Kasap

Typical solar cells are made of the same material so that the pn junction is a homojunction. Some solar cell materials and their efficiencies are summarized in Table 1. A comprehensive state of current research in different solar cell technologies and their efficiency is available in *Figure 15*. Heterojunction solar cells are also possible and they have the advantage of minimizing absorption in regions other than the depletion region, but overall cost increases because of the use of different materials and the tight processing conditions needed to produce defect free interfaces. A schematic of such a cell based on GaAs/AlGaAs is shown in Figure *16*. The shorter wavelengths are absorbed by the AlGaAs layers while the longer wavelengths, with higher penetration depths, are absorbed by the GaAs layer. This leads to an overall efficiency of around 25%, see Table 1. It is also possible to have a homojunction solar cell but with a passivating layer of another material at the surface to reduce defects. This is shown in Figure 17. The surface passivating layer removes the dangling bonds and minimizes carrier trapping. The passivation layer is a thin layer of a higher band gap material to minimize absorption. Similarly, amorphous semiconductor materials like Si and Ge also have a passivating layer of H, a-Si:H or a-Ge:H, to reduce dangling bonds. Another way of improving solar cell efficiency is to have more than one cell in tandem. These are called tandem solar cells and a schematic is shown in Figure 18.

These consist of two pn junction solar cells, with the first one having a higher band gap than the second. Thus, the shorter wavelengths can be absorbed in cell 1, see Figure 18, while the longer wavelengths are absorbed in cell 2. The advantage is that a larger portion of the solar radiation is used so that tandem cells have high efficiency, see Table 1, but it also adds a layer of complexity in growth and increases cost. Tandem cells can also be made using amorphous Si:H and Ge:H. These are cheaper to make and more efficient than individual amorphous solar cell devices.

Table 1 : Some common solar cell materials and their characteristics. Adapted from Principles of Electronic Materials - S.O. Kasap

Semiconductor	E_g ***(eV)***	V_{oc} ***(V)***	J_{sc} ***(mA cm^{-2})***	***η (%)***
Si, single crystal	1.1	0.55-0.7	42	16-24
Si, polycrystaline	1.1	0.5-0.65	38	12-19
Amorphous Si:Ge:H film				8-13
GaAs, Single crystal	1.42	1.02	28	24-25
GaAIAs/GaAs, tandem		1.03	27.9	25
GaInP/GaAs, tandem		2.5	14	25-30
CdTe, Thin film	1.5	0.84	26	15-16
InP, single crystal	1.34	0.87	29	21-22
$CuInSe_2$	1.0			12-13

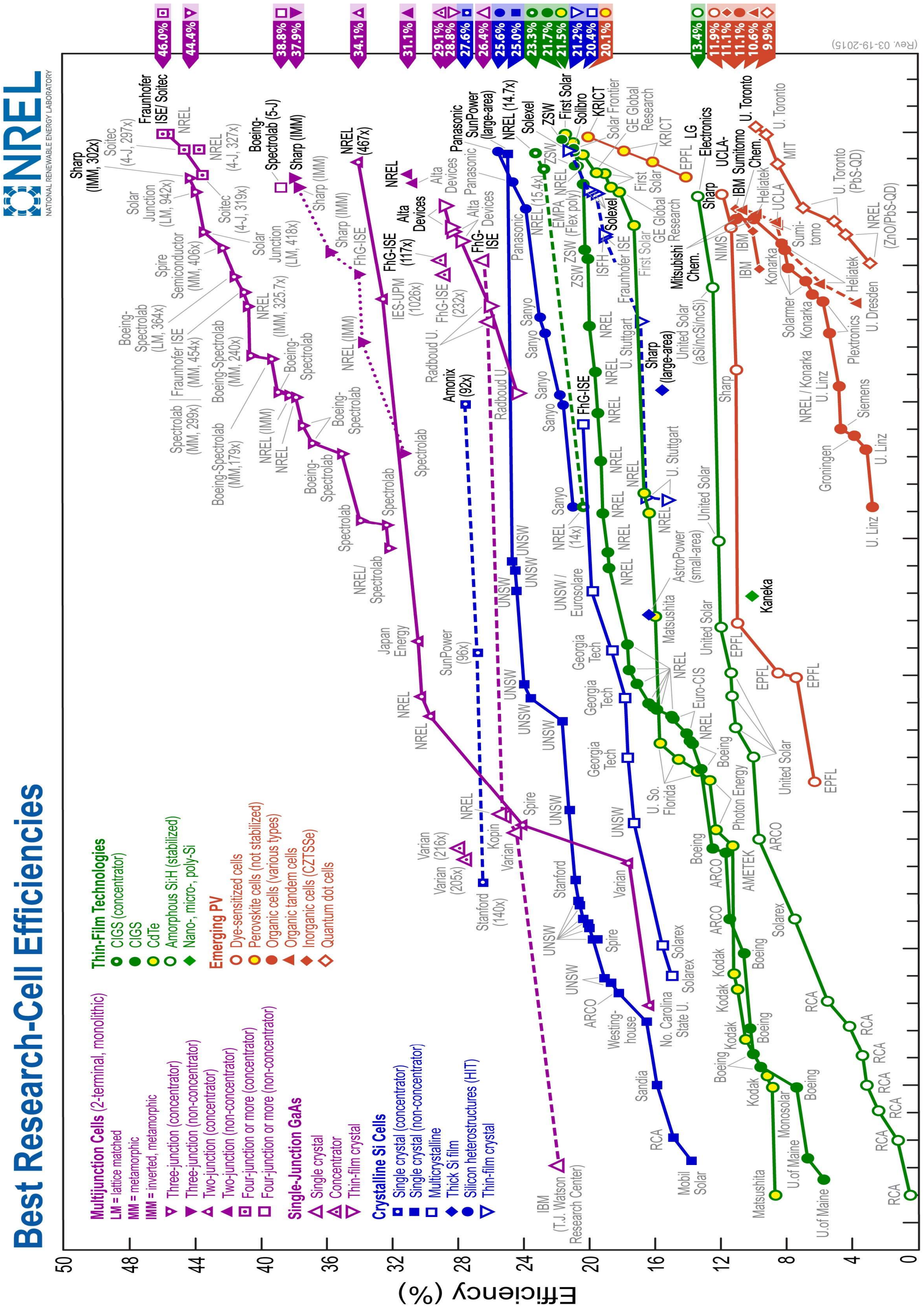

Figure 15. Efficiency of various research solar cells. The latest diagram is available at http://www.nrel.gov/ncpv/

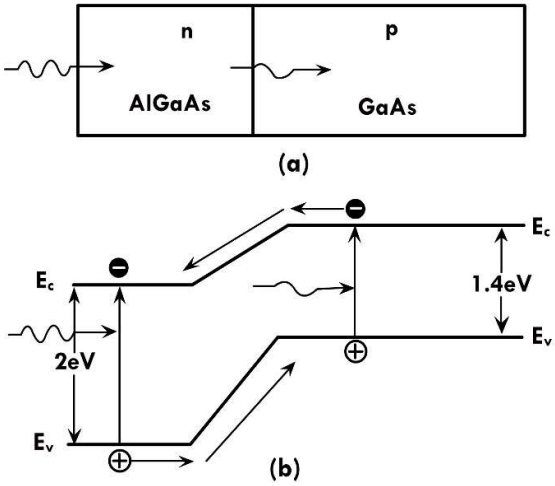

Figure 16. (a) GaAs/AlGaAs based heterojunction solar cell. (b) Energy band alignment across the junction. AlGaAs has the higher band gap and can absorb higher energy radiation while GaAs can absorb the lower energy portion of the solar spectrum. Adapted from Principles of Electronic Materials - S.O. Kasap

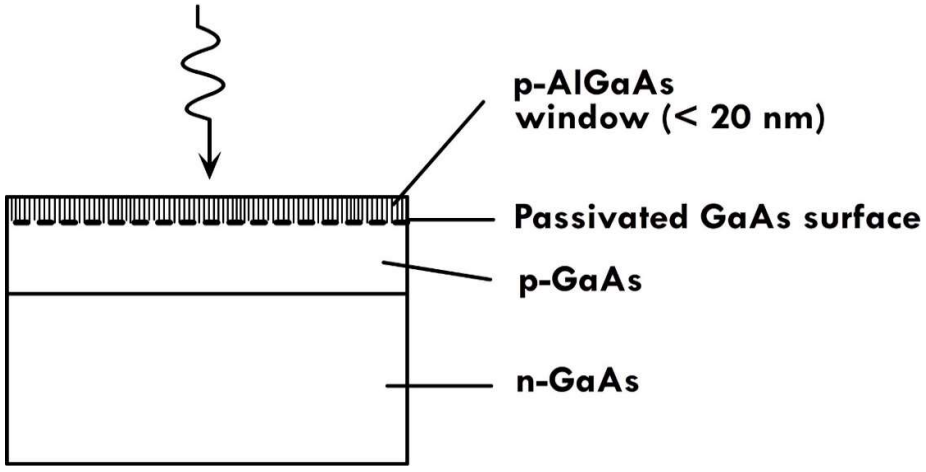

Figure 17. Schematic of a GaAs based homojunction solar cell with a surface passivating layer to minimize surface recombination. This layer shouldbe thin and have a high band gap to minimize absorption. Adapted from *Principles of Electronic Materials - S.O. Kasap*

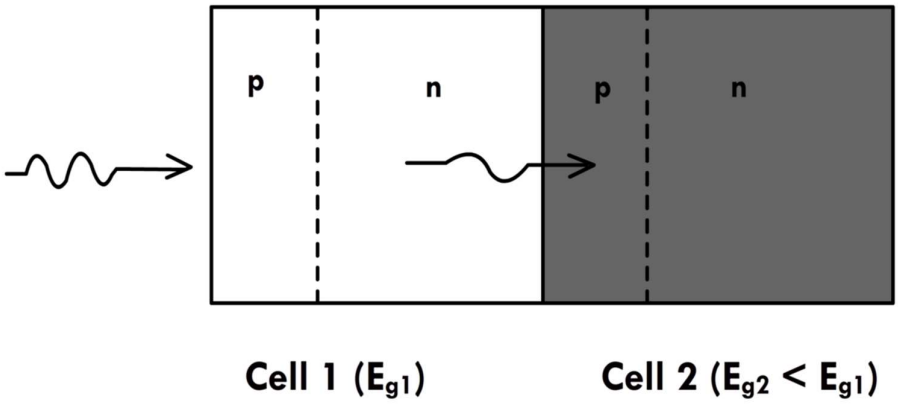

Figure 18. Tandem solar cells. The higher band gap cell is closer to the illuminating surface to absorb the short wavelengths and the smaller bandgap cell is at the interior to absorb the longer wavelengths. Adapted from *Principles of Electronic Materials - S.O. Kasap*

Materials and Methodology

Device methodology and simulation parameters:

Using the SCAPS-1D simulation programme, the perovskite solar cell characteristics were designed and analysed in the current work [5]. The devices in our investigation are simulated using SCAPS-1D software. The suggested device's structure is Glass/ITO/WS_2/$CH_3NH_3PbI_3$/P3HT/Au, as demonstrated in Figure 19. Structure of perovskite solar cell. In this cell structure, Light beams fall on indium tin oxide (ITO), which serves as a front contact. The n-type Tungsten disulphide (WS2) contacts that are formed on ITO serve as an electron transport layer. A layer of 3-hexylthiophene-2,5-diyl (P_3HT), which is used as the HTL, is placed above the perovskite methyl ammonium lead iodide ($CH_3NH_3PbI_3$) and serves as an absorber layer. Contact has been backed with gold (Au). To achieve their maximum values and to enhance the performance of perovskite solar cells, the simulation method adjusted the characteristics of PV cells including thickness, band gap, acceptor density, and absorber temperature while holding all other factors constant.

Simulation parameters:

Table *2* provides a list of the input parameters that were used to describe the fundamental of the n-i-p planer heterojunction structure of the Glass/ITO/WS_2/$CH_3NH_3PbI_3$/P_3HT/Au device. The work functions for the front and rear contacts were assumed to be 5.1 eV and 4.2 eV, respectively. We selected a single energy distribution and a capture cross-section of 1 x 10^{-15} cm^2 in our modelling study, along with neutral defects for electrons and holes. The simulations were run at an operating temperature of 300 K with AM1.5 G illumination.

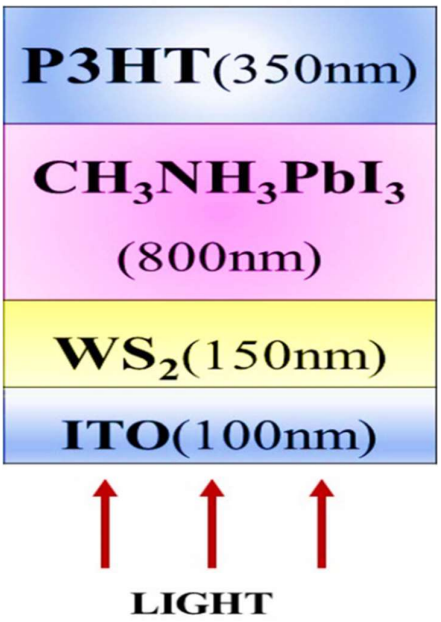

Figure 19. Structure of perovskite solar cell.

Table 2 : Parameters of different layers of solar cell [*12–14,18–21*]

Parameters	P3HT	$CH_3NH_3PbI_3$	WS_2	ITO
Thickness (μm)	0.350	0.800	0.150	0.100
Bandgap (eV)	1.700	1.610	1.800	3.500
Electron affinity (eV)	3.500	3.860	3.950	4.000
Dielectric Permittivity	3.000	6.500	13.600	9.000
N_c (1/cm^3)	2.0×10^{18}	2.2×10^{18}	2.2×10^{17}	2.2×10^{18}
N_v (1/cm^3)	2.0×10^{19}	1.8×10^{18}	2.2×10^{16}	1.8×10^{18}
Electron Thermal velocity (cm s^{-1})	1.0×10^7	10^7	10^7	10^7
Hole Thermal Velocity (cm s^{-1})	10^7	10^7	10^7	1.0×10^7
Electron Mobility (cm^2 V^{-1} s^{-1})	1.8×10^{-3}	2.0	1.0×10^2	2.0
Hole Mobility (cm^2 V^{-1} s^{-1})	1.8×10^{-2}	2.0	1.0×10^2	1.0
N_D (1/cm^3)	—	1.0×10^{14}	1.0×10^{18}	2.0×10^{19}
N_A(1/cm^3)	1.0×10^{19}	1.0×10^{14}	—	—
N_t (1/cm^3)	1.0×10^{15}	2.5×10^{12}	1.0×10^{15}	1.0×10^{16}

Numerical method:

The numerical analysis is performed using SCAPS-1D software. Different curves have been plotted and an analysis of the curve is done. The spectral response and EFD (Electric field distribution) can be determined by solving Poisson's(*7*) and the continuity equations for the charge carriers as in equations (8) and (9) and *For holes*,), respectively [19,22]

$$\frac{d}{dx}\left(-\varepsilon(x)\frac{d\varphi}{dx}\right) = [p(x) - n(x) + N_D(x) - N_A(x) + p(x) - n(x)] \tag{7}$$

Where, p represents free hole density, N_A represents acceptor density, N_D represents donor density, n(x) and p(x) represent electron and hole density and ε is the medium's dielectric constant. The equation of continuity retains the passage of all the charge carriers in terms of motion, generation and recombination. The continuity equation of electrons and holes is specified by [23]

For electrons, $$\frac{\partial n(x,t)}{\partial t} = \frac{1}{q}\frac{\partial J_n}{\partial x} + G_n(x,t) - R_n(x,t) \tag{8}$$

For holes, $$\frac{\partial p(x,t)}{\partial t} = \frac{1}{q}\frac{\partial J_p}{\partial x} + G_p(x,t) - R_p(x,t) \tag{9}$$

Carrier density of electrons and holes J_n and J_p, respectively can be shown as:

$$J_n = q\left[nu_nE + D_n\frac{dn}{dx}\right] \tag{10}$$

Where D_n is the diffusion constant of the electron.

$$J_p = q\left[nu_pE + D_p\frac{dp}{dx}\right] \tag{11}$$

Where D_p is diffusion constant of the hole.

For the condition of steady-state $\frac{dn}{dt} = 0$ and $\frac{dp}{dt} = 0$

$$\frac{1}{q}\frac{\partial J_n}{\partial x} = -G_n(x,t) + R_n(x,t) \tag{12}$$

Where G_n and R_n are the generation and recombination rate of an electron, respectively. Poisson's equation describes how photovoltaic devices behave in terms of electric charge density, electric field, voltage, and free charge carrier density. For

different donor and doping concentrations, this equation has been explained [24]. Substituting the value of J_n from the above equation, we have:

$$nu_n \frac{dE}{dx} + u_n E + \frac{dn}{dx} + D_n \frac{d^2 n}{dx^2} = -G_n(x) + R_n(x) \tag{13}$$

$$-pu_p \frac{dE}{dx} - u_p E \frac{dn}{dx} + D_p \frac{d^2 p}{dx^2} = -G_p(x) + R_p(x) \tag{14}$$

Where, G_p and R_p is the generation and recombination rate of the hole, respectively. Using SCAPS-1D these differential equations can be solved.

Result and discussion:

Band arrangement of simulated cell structure:

Using the SCAPS-1D simulation program, we modelled a device structure of ITO/WS2/$CH_3NH_3PBI_3$/P3HT/Au. The band diagram of the proposed simulated device structure has been depicted in *Figure 21*. The parameters used for the study are shown *Table 2*. In this device structure, the absorber layer has been given thickness of 350 nm (CH3NH3PbI3), while the HTL is treated with P3HT with a thickness of 350 nm and WS2 as an ETL with a thickness of 150 nm. From Figure 21, it has been observed that both conduction and valence band offsets (VBO) of the P3HT/$CH_3NH_3PbI_3$ are 0.36 eV and 0.27 eV while for $CH_3NH_3PbI_3$/WO_3 are 0.21 eV and 0.28 eV, respectively. In Figure 20, SCAPS-1D simulator used show the input panel to start defining the solar cell different layers.

Figure 20. SCAPS-1D simulator used show the input panel to start defining the solar cell different layers

Influence of variation in thickness of absorber layer

The effect of variation of thickness of $CH_3NH_3PbI_3$ (active layer) on solar cell performance can be visualized in Figure *22*. The simulation results imply as perovskite thickness varies, the electrical performance of the solar cell is also modified in Figure *22*(a), it is shown that the PCE increases and becomes maximum at 1.3 μm absorber

($CH_3NH_3PbI_3$) thickness as more light absorption and efficiency rises because of the generation and recombination of electrons and holes, after that with further increase in thickness, the efficiency slightly reduces [13].In Figure *22*(b),V_{OC} goes up rapidly with the increasing thickness of the perovskite layer. In Figure *22*(c), it is observed that on increasing thickness of $CH_3NH_3PbI_3$ absorber, J_{SC} increases because, in perovskite layer of higher thickness, incident light having higher wavelength are absorbed which results in increment in carrier production. Figure *22*(d) illustrates as the thickness of an active layer increases due to an increase in series resistance, the fill factor (FF) decreases.

Effect of variation in the bandgap of absorber layer on device parameters

A perovskite solar photovoltaic device's band gap is an essential limit, therefore changes in it affect the device's efficiency. The bandgap has been adjusted in this simulation to range between 1.3 and 2.3 eV as seen in Figure *23*. As illustrated in Figure *23* (a), It is shown that PCE decreases as the bandgap increases[10]. This is due to the fact that increasing the bandgap lowers the number of photons that are absorbed while raising the energy at which they can be extracted. In Figure *23* (b), the V_{OC} has an ideal value when the bandgap is between 1.5–1.7 eV and later on, as the material's bandgap is increased, it somewhat reduces.

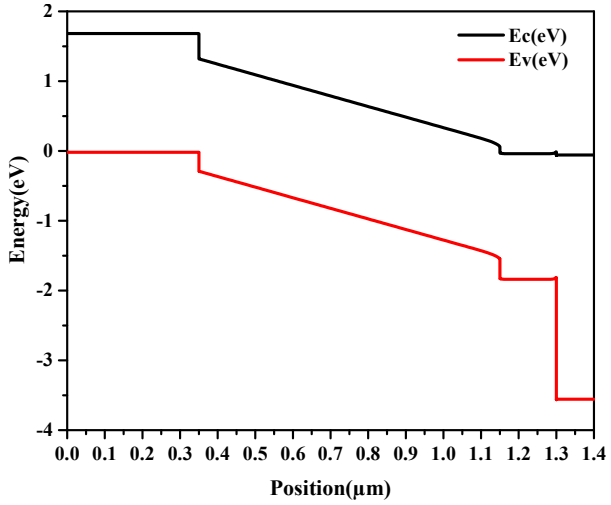

Figure 21. Band arrangement of the cell structure.

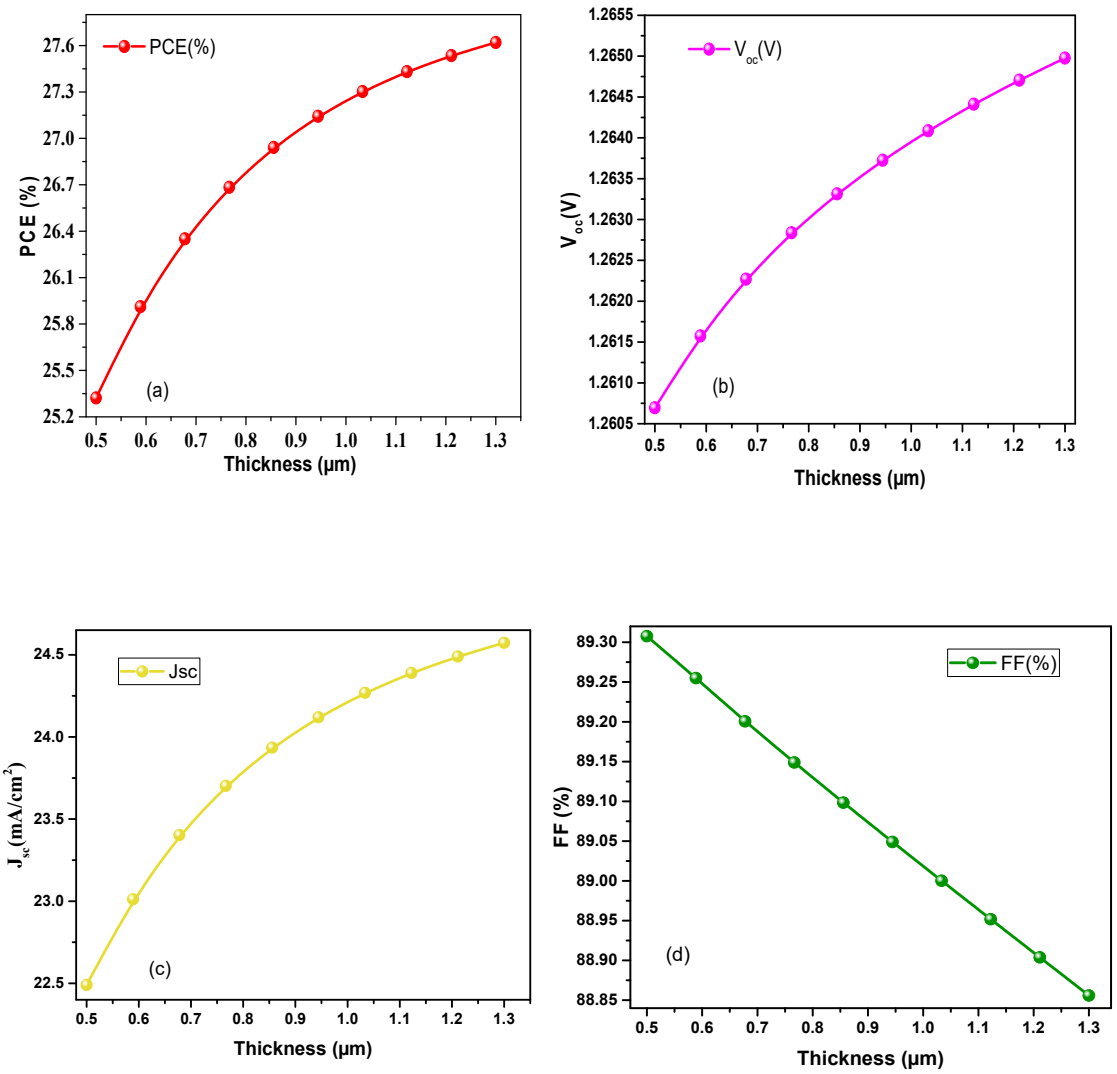

Figure 22. (a)–(d) Influence of variation in perovskite's thickness on solar cell parameters.

In Figure *23* (c), It is shown that when the bandgap increases, the higher energy photons' absorption reduces, and the J_{SC} gradually falls. The FF increases on increasing band gap to 1.95 eV as depicted in Figure *23* (d) and then there is a sudden drop in FF because of a decrement in photons' absorption with lower energy than the band gap energy. Higher-energy photons that collide with the object and produce photocurrent.

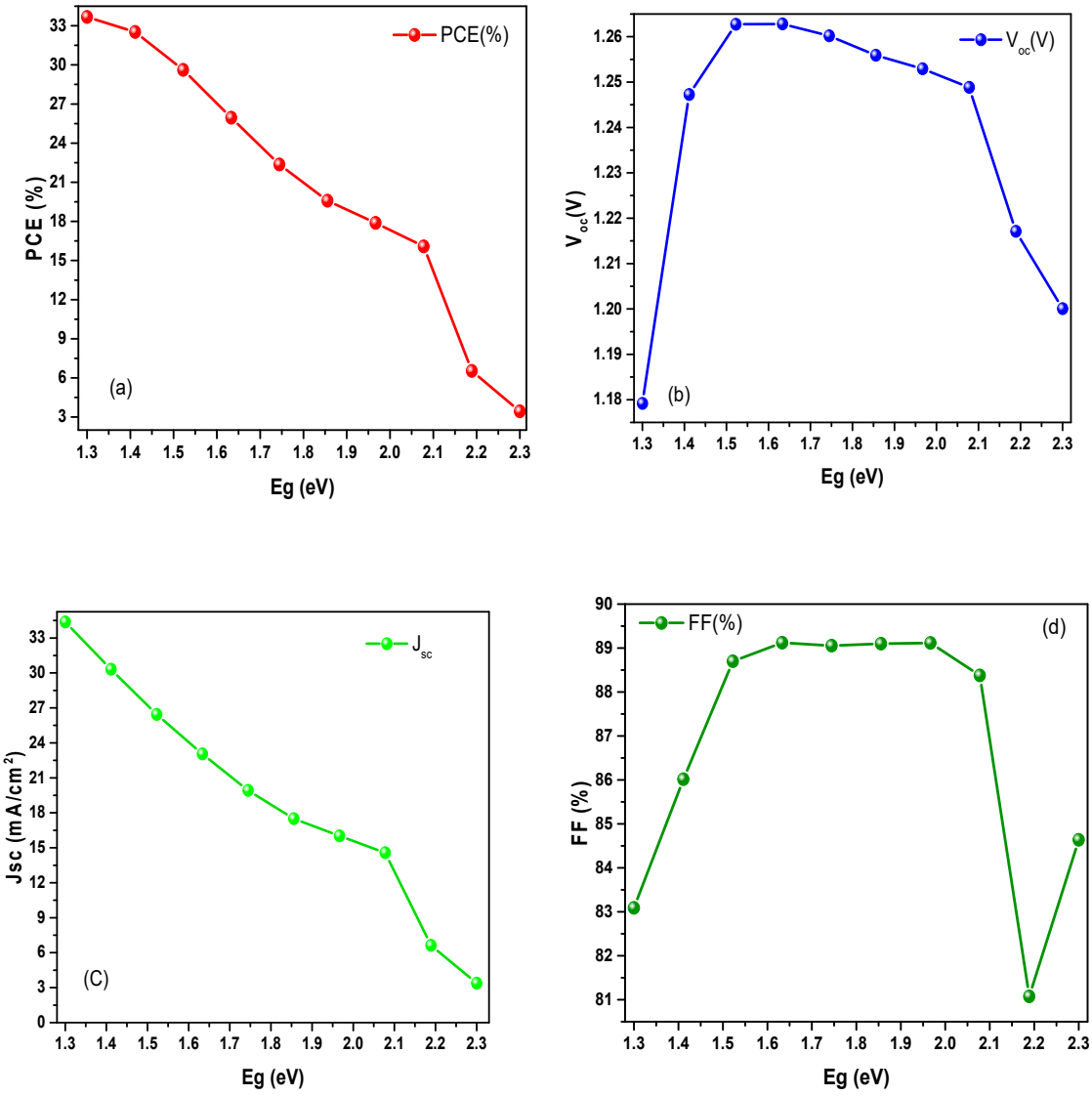

Figure 23. (a)–(d) Impact of the bandgap of the absorber layer on the device parameters.

Impact of variation in doping concentration of absorber layer

To optimize solar performance and improve efficiency, the active layer doping concentration is essential. To assess how the acceptor density of an absorber layer affects cell performance, the acceptor concentration was varied from 1×10^{13} cm^{-3} to 1×10^{22} cm^{-3}, and device parameters such as V_{OC}, J_{SC}, FF, and PCE were examined, which is shown in Figure *24* [12]. From Figure *24*, it is observed that on increasing the doping concentration of an active layer, FF, V_{OC} and PCE are constant up to 1×10^{17} cm^{-3}. Additionally, as acceptor density rises, solar cell performance rises and J_{SC}

(short-circuit current density) falls. The open-circuit voltage (V_{OC}) increases with acceptor density from 1×10^{17} cm^{-3} to 1×10^{22} cm^{-3} and the maximum V_{OC} is obtained as 1.5907 V at 1×10^{22} cm^{-3}. The current density (J_{SC}) is found to be 23.795 mA cm^{-2} at 1×10^{13} cm^{-3} and decreases to 20.22 mA cm^{-2} at 1×10^{22} cm^{-3}. Fill Factor (FF) is constant up to 1×10^{15} cm^{-3} and after that abruptly rises up to 1×10^{21} cm^{-3} since, upon an increase in the doping concentration of the acceptor atom, cell resistance decreases.

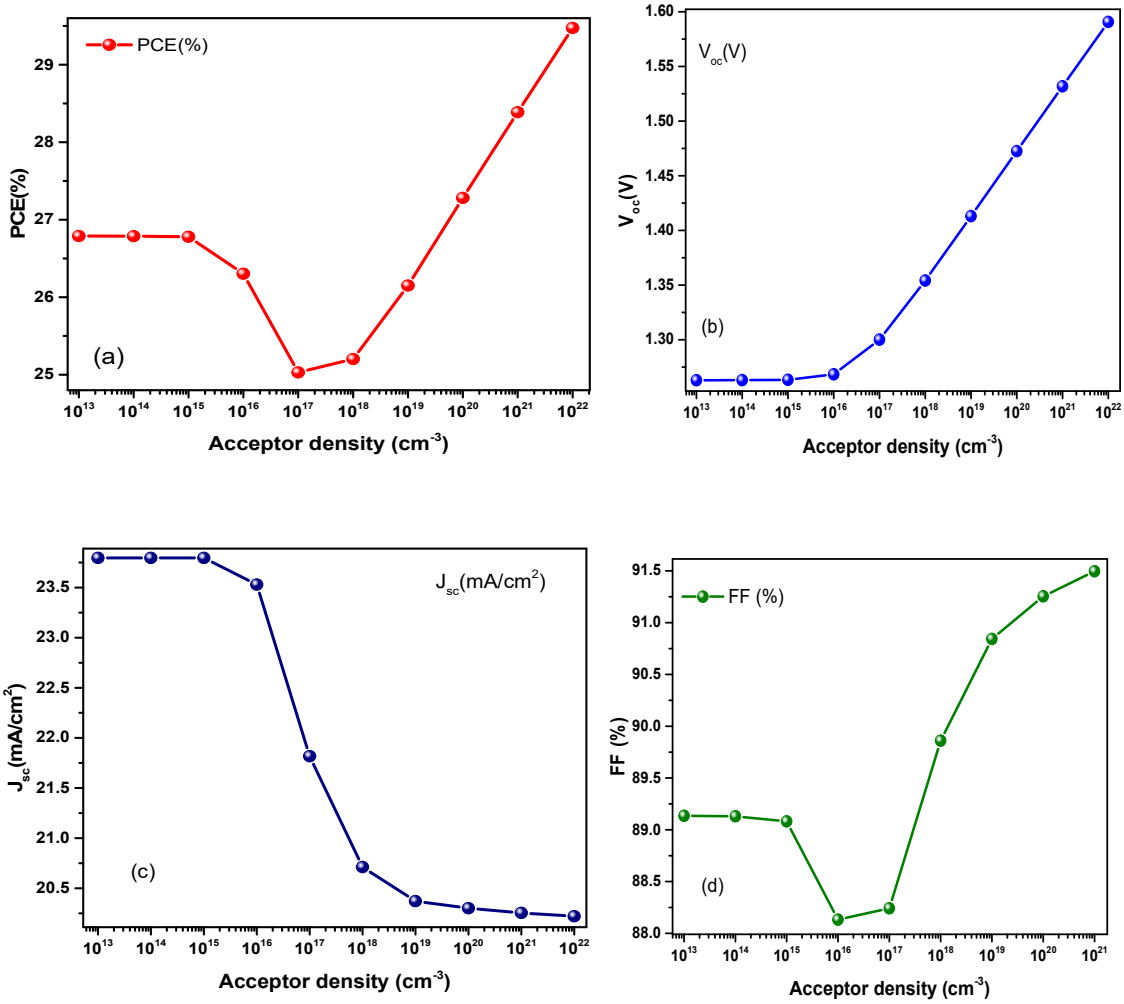

Figure 24. (a)–(d) Consequence of acceptor density of active layer on the device parameters.

Following acceptor doping, holes and electrons will invariably behave as majority and minority carriers, respectively. Thus, at particular doping of the acceptor atom, the number of hole majority carriers increases which increases the FF of the

device. The gained PCE of the photovoltaic cell at 1×10^{13} cm^{-3} is 26.788% and 29.73% at 1×10^{22} cm^{-3} after that on increasing doping concentration, PCE (Power Conversion Efficiency) slightly decreases up to 25.03% at a concentration of 1×10^{17} cm^{-3}. In this simulation study, to achieve optimum photovoltaic cell performance, a minimal acceptor density of 1×10^{14} cm^{-3} has been chosen. Increased acceptor density of perovskite decreases the depletion gap and increases the electric field. The increase in V_{OC} of the device is due to the recombination of carriers which also leads to a gain in power conversion efficiency (η). The equation can also explain the increase in V_{OC} increasing the acceptor density (N_A)

$$V_{OC} = \frac{E_g}{q} - \frac{kT}{q} ln \left[\frac{qD_e N_c N_v}{J_{SC} N_A L_n}\right] \quad (15)$$

Where, k denotes the Boltzmann constant, E_g denotes the bandgap energy, T denotes absolute temperature in Kelvin (K), D_e is the diffusion current of e^-, N_C and N_V represent the density of states of conduction and valence band, respectively. N_A stands for doping acceptor density, J_{sc} for short circuit current density and L_n denotes electron diffusion length [25].

Influence of varying temperature on solar cell parameters

The influence of temperature on the solar cell's efficiency has been discussed in this subsection. Solar cells are placed in open regions where the temperature is too high. The variation in temperature influences the device's parameters. With the temperature rise, the mobility, band gap, and carrier concentration of electrons and holes of the device will also vary. The efficiency and all other photovoltaic properties of the device drop as the temperature rises. This could be the result of the defect density in the layers increasing with temperature, resulting in a decrease in efficiency. The deformation stress rises with temperature, which could also cause a decrease in the efficiency of the device. The device's FF and efficiency are decreased because the temperature affects the diffusion length, which causes the series resistance to increase. Additionally, a rise in temperature causes a rise in saturation current, which raises the recombination rate and lowers the FF value. A higher photocurrent results from the bandgap narrowing and rising thermal energy of electrons as the temperature rises. But according to the proposed device configuration, J_{sc} doesn't change when the temperature rises. The overall PCE is decreased because of the significant V_{oc} loss caused by the temperature increase [26]. The effect of temperature on the PSC's

photovoltaic performance has been investigated, as illustrated in Figure 25. The thickness of the perovskite is 0.8 μm with a defect density of 2.5×10^{12} cm^{-3} and that of WS2 (ETL) is 0.15 μm with a defect density of 1.0×10^{15} cm−3. Usually, in this simulation work, the temperature has been set from 250 K–300 K to see how raising the operating temperature affects the cell's performance [27].

On increasing the operating temperature, V_{OC} falls abruptly from 1.29 V to 1.26 V as depicted in Figure 25(b). Also, PCE declines on an increase in the operating temperature as the reverse saturation current increases. At operating temperatures of 250 K—300 K efficiency of 27.84% to 26.78% are obtained [25, 28,29,30]. FF decreases from 90.57% to 89.129%. It has been observed that J_{SC} increases on increasing temperature. The operating temperature of the device has been set to 300 K. To check the device performance the temperature has been varied from 250K–300K, and we observed that on increasing the operating temperature, the device performance is decreasing. Therefore, the operating temperature has been chosen as 300 K.

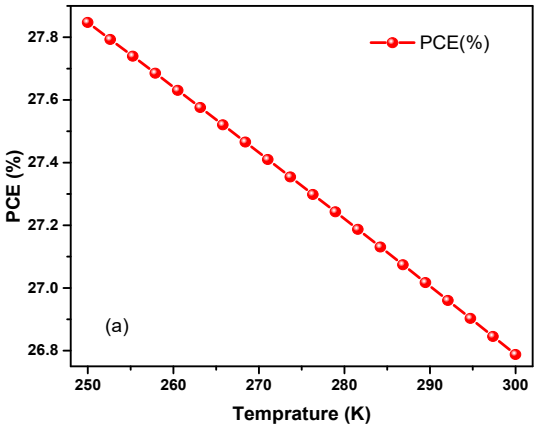

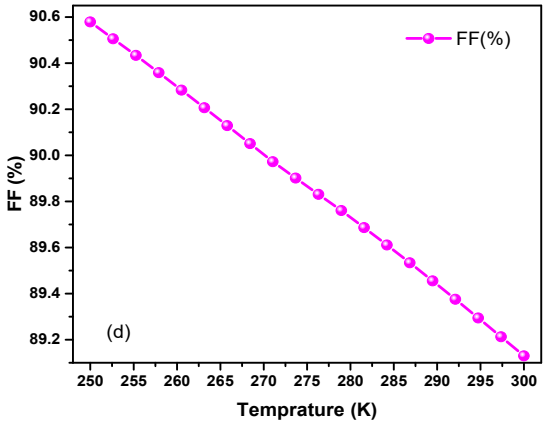

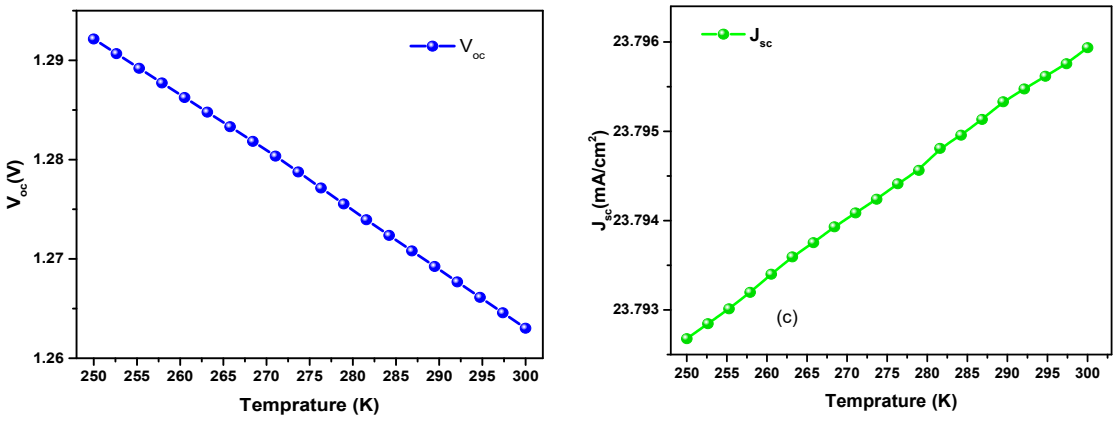

Figure 25. (a)–(d) Influence of temperature of perovskite on the device parameters.

Optimized QE and J-V characteristics of cell performance

The characteristics of current density, voltage (J-V) and quantum efficiency (QE) has been examined in the planned cell architecture. Using optimized values of parameters like thickness, bandgap, acceptor density and temperature of the solar device, the optimized performance of the device has been obtained from the simulation results. The simulation resulted in a Power Conversion Efficiency (PCE) of 28.38%, short-circuit current density (J_{SC}) of 21.86 mA cm^{-2}, fill factor (FF) of 90.93% and an open-circuit voltage (V_{OC}) of 1.4275 V. The PCE and FF of the PSC studied in this work are 28.38% and 90.93% which is the maximum as compared to other devices reported on a date [31]. Figure 26 shows the current density and voltage characteristics, as well as the quantum efficiency (QE) curve, indicating improved solar cell performance.

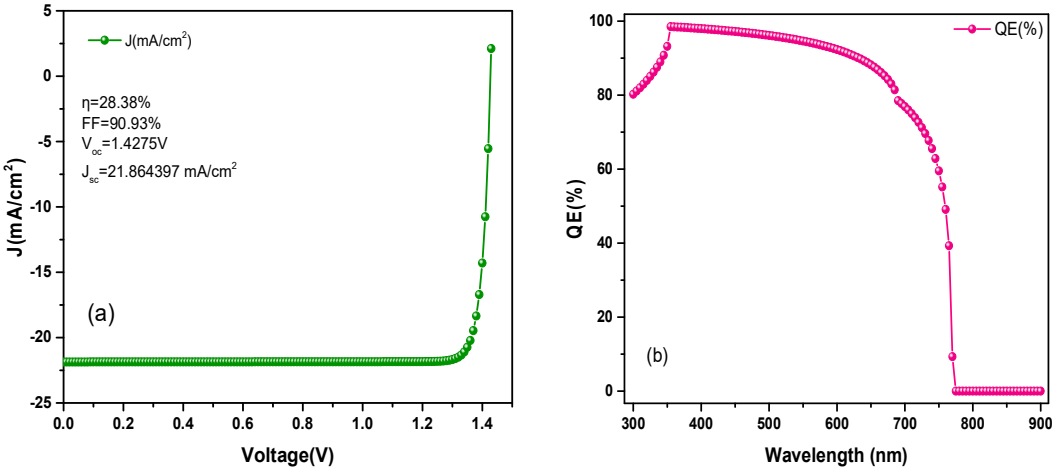

Figure 26. (a) J-V curve of cell performance and (b) QE of optimized device performance.

Conclusions

In the present study, the perovskite solar cell of device architecture ITO/WS_2/$CH_3NH_3PbI_3$/P3HT/Au is simulated by using a SCAPS-1D simulator program. The simulation study of lead-based $CH_3NH_3PbI_3$ perovskites solar cells shows that the performance of the device highly depends on the thickness of the absorber layer, work function and back and front contact materials. Further, the various parameters such as defect density, doping density of acceptor and donor atom and temperature play a significant role in the performance of the perovskite solar cell. All of the parameters that affect the performance of the perovskite solar cell are optimized to increase efficiency. The studied perovskite solar cell has the highest efficiency of 28.38%. Perovskites with a bandgap of 1.6 - 1.7 eV should be employed as an active layer to achieve good photovoltaic performance. Our research reveals that using a thin layer reduces photocurrent due to lesser absorption, but carrier extraction is significant. Although greater absorption increases the number of carriers in the device while recombination reduces V_{OC} for thick perovskite layers which results in lower collection efficiency.

Acknowledgments

We are thankful to Dr. Burgelman and his team, the Department of Electronics and Information Systems University of Gent Belgium for developing SCAPS -1D tool.

I express my deep gratitude, regard to my supervisor, Dr. Swapan Kumar Mandal, for his constant encouragement and valuable suggestions. I would have made no progress without his help and support.

I would like to convey my heartfelt gratitude to Paramesh Chandra (Ph.D. Scholar, Visva-Bharati), my mentor, for his invaluable advice and assistance in completing my project.

I thank my classmate Saikat Samadder for his assistance in different ways.

I am really grateful to my family for their constant support and encouragement.

References

1. Al-Mousoi, A. K. *et al.* Simulation and analysis of lead-free perovskite solar cells incorporating cerium oxide as electron transporting layer. *RSC Adv.* **12**, 32365–32373 (2022).

2. Husainat, A., Ali, W., Cofie, P., Attia, J. & Fuller, J. Simulation and Analysis of Methylammonium Lead Iodide ($CH_3NH_3PbI_3$) Perovskite Solar Cell with Au Contact Using SCAPS 1D Simulator. *Am. J. Opt. Photonics* **7**, 33 (2019).

3. Frost, J. M. *et al.* Atomistic origins of high-performance in hybrid halide perovskite solar cells. *Nano Lett.* **14**, 2584–2590 (2014).

4. Baikie, T. *et al.* Synthesis and crystal chemistry of the hybrid perovskite (CH3NH3)PbI3 for solid-state sensitised solar cell applications. *J. Mater. Chem. A* **1**, 5628–5641 (2013).

5. Lin, L., Jiang, L., Qiu, Y. & Fan, B. Analysis of Sb2Se3/CdS based photovoltaic cell: A numerical simulation approach. *J. Phys. Chem. Solids* **122**, 19–24 (2018).

6. He, Y., Xu, L., Yang, C., Guo, X. & Li, S. Design and Numerical Investigation of a Lead-Free Inorganic Layered Double Perovskite Cs4CuSb2Cl12 Nanocrystal Solar Cell by SCAPS-1D. *Nanomaterials* **11**, 2321 (2021).

7. Purcar, V. *et al.* Degradation of TiO2 and/or SiO2 hybrid films doped with different cationic dyes. *Thin Solid Films* **534**, 301–307 (2013).

8. Samiul Islam, M. *et al.* Defect Study and Modelling of SnX3-Based Perovskite Solar Cells with SCAPS-1D. *Nanomaterials* **11**, 1218 (2021).

9. Yoo, J. J. *et al.* Efficient perovskite solar cells via improved carrier management. *Nature* **590**, 587–593 (2021).

10. Khattak, Y. H., Baig, F., Shuja, A., Beg, S. & Soucase, B. M. Numerical analysis guidelines for the design of efficient novel nip structures for perovskite solar cell. *Sol. Energy* **207**, 579–591 (2020).

11. Srivastava, P. *et al.* Theoretical study of perovskite solar cell for enhancement of device performance using SCAPS-1D. *Phys. Scr.* **97**, 125004 (2022).

12. Burgelman, M., Nollet, P. & Degrave, S. Modelling polycrystalline semiconductor solar cells. *Thin Solid Films* **361–362**, 527–532 (2000).

13. Rai, S., Pandey, B. K. & Dwivedi, D. K. Device simulation of low cost HTM free perovskite solar cell based on TiO2 electron transport layer. in 140022 (2020). doi:10.1063/5.0001230.

14. Sunny, A., Rahman, S., Khatun, Most. M. & Ahmed, S. R. A. Numerical study of high performance HTL-free CH3NH3SnI3-based perovskite solar cell by SCAPS-1D. *AIP Adv.* **11**, 065102 (2021).

15. Kung, P.-K. *et al.* A Review of Inorganic Hole Transport Materials for Perovskite Solar Cells. *Adv. Mater. Interfaces* **5**, 1800882 (2018).

16. Casas, G. A., Cappelletti, M. A., Cédola, A. P., Soucase, B. M. & Peltzer y Blancá, E. L. Analysis of the power conversion efficiency of perovskite solar cells with different materials as Hole-Transport Layer by numerical simulations. *Superlattices Microstruct.* **107**, 136–143 (2017).

17. Photovoltaic materials: Present efficiencies and future challenges | Science. https://www.science.org/doi/10.1126/science.aad4424.

18. Sharma, D., Mehra, R. & Raj, B. *Mathematical Modelling And Simulation of CH3NH3Pb(I1-Xbrx)3 Based Perovskite Solar Cells For High Efficiency*. (2021). doi:10.21203/rs.3.rs-1133949/v1.

19. Lin, L. *et al.* Boosting efficiency up to 25% for HTL-free carbon-based perovskite solar cells by gradient doping using SCAPS simulation. *Sol. Energy* **215**, 328–334 (2021).

20. Rai, N., Rai, S., Singh, P. K., Lohia, P. & Dwivedi, D. K. Analysis of various ETL materials for an efficient perovskite solar cell by numerical simulation. *J. Mater. Sci. Mater. Electron.* **31**, 16269–16280 (2020).

21. Deepthi Jayan, K. & Sebastian, V. Comprehensive device modelling and performance analysis of MASnI3 based perovskite solar cells with diverse ETM, HTM and back metal contacts. *Sol. Energy* **217**, 40–48 (2021).

22. Sadanand, Singh, P. K., Rai, S., Lohia, P. & Dwivedi, D. K. Comparative study of the CZTS, CuSbS2 and CuSbSe2 solar photovoltaic cell with an earth-abundant non-toxic buffer layer. *Sol. Energy* **222**, 175–185 (2021).

23. Simya, O. K., Mahaboobbatcha, A. & Balachander, K. Compositional grading of CZTSSe alloy using exponential and uniform grading laws in SCAPS-ID simulation. *Superlattices Microstruct.* **92**, 285–293 (2016).

24. Bhattarai, S., Sharma, A. & Das, T. D. Efficiency enhancement of perovskite solar cell by using doubly carrier transport layers with a distinct bandgap of MAPbI3 active layer. *Optik* **224**, 165430 (2020).

25. Rai, S., Pandey, B. K., Garg, A. & Dwivedi, D. K. Hole transporting layer optimization for an efficient lead-free double perovskite solar cell by numerical simulation. *Opt. Mater.* **121**, 111645 (2021).

26. Bhardwaj, K. S., Rai, S., Sadanand, Lohia, P. & Dwivedi, D. K. Investigating the performance of mixed cation mixed halide-based perovskite solar cells using various hole-transport materials by numerical simulation. *Opt. Quantum Electron.* **53**, 602 (2021).

27. Gan, Y. *et al.* Numerical Investigation Energy Conversion Performance of Tin-Based Perovskite Solar Cells Using Cell Capacitance Simulator. *Energies* **13**, 5907 (2020).

28. Bouich, A. *et al.* Experimental, theoretical, and numerical simulation of the performance of CuInxGa(1-x) S2-based solar cells. *Optik* **183**, 137–147 (2019).

29. Heriche, H., Rouabah, Z. & Bouarissa, N. New ultra thin CIGS structure solar cells using SCAPS simulation program. *Int. J. Hydrog. Energy* **42**, 9524–9532 (2017).

30. Rahman, S. & Ahmed, S. R. A. Photovoltaic performance enhancement in CdTe thin-film heterojunction solar cell with Sb2S3 as hole transport layer. *Sol. Energy* **230**, 605–617 (2021).

31. Best Research-Cell Efficiency Chart. https://www.nrel.gov/pv/cell-efficiency.html.